

DOE/BC/15311-4  
(OSTI ID: 777917)

POROSITY AND PERMEABILITY EVOLUTION ACCOMPANYING  
HOT FLUID INJECTION INTO DIATOMITE

SUPRI TR-123  
March 2001

By:  
I. Diabira  
L.M. Castanier  
A.R. Kavscek

Date Published: April 2001

Work Performed Under Contract No. DE-FC26-00BC15311

Stanford University  
Stanford, California



**National Energy Technology Laboratory  
National Petroleum Technology Office  
U.S. DEPARTMENT OF ENERGY  
Tulsa, Oklahoma**

## **DISCLAIMER**

This report was prepared as an account of work sponsored by an agency of the United States Government. Neither the United States Government nor any agency thereof, nor any of their employees, makes any warranty, expressed or implied, or assumes any legal liability or responsibility for the accuracy, completeness, or usefulness of any information, apparatus, product, or process disclosed, or represents that its use would not infringe privately owned rights. Reference herein to any specific commercial product, process, or service by trade name, trademark, manufacturer, or otherwise does not necessarily constitute or imply its endorsement, recommendation, or favoring by the United States Government or any agency thereof. The views and opinions of authors expressed herein do not necessarily state or reflect those of the United States Government.

This report has been reproduced directly from the best available copy.

DOE/BC/15311-4  
Distribution Category UC-122

Porosity and Permeability Evolution Accompanying Hot Fluid Injection Into Diatomite

SUPRI TR—123

By  
I. Diabira  
L.M. Castanier  
A.R. Kavscek

April 2001

Work Performed Under Contract DE-FC26-00BC15311

Prepared for  
U.S. Department of Energy  
Assistant Secretary for Fossil Energy

Thomas Reid, Project Manager  
National Petroleum Technology Office  
P.O. Box 3628  
Tulsa, OK 74101

Prepared by  
Stanford University  
Department of Petroleum Engineering  
Green Earth Sciences Building, Room 080b  
367 Panama Street  
Stanford, CA 94305-2220

## Table of Contents

	<b><u>Page</u></b>
List of Tables	iii
List of Figures	iii
Acknowledgements	iv
Abstract	v
1. Introduction	1
2. Experimental Apparatus	3
3. Experimental Procedure	5
3.1 Design	5
3.2 Procedure	7
3.3 Analysis	8
4. Experimental Results	9
5. Discussion	11
6. Conclusions	14
Nomenclature	16
References	18

## List of Tables

	<u>Page</u>
1. Summary of experimental conditions	20
2. Summary of apparent compressibility from flow experiments	20

## List of Figures

	<u>Page</u>
1. Schematic of experimental apparatus	21
2. Schematic of core assembly	22
3. Permeability versus time (left) and porosity profiles (right) for core 1	23
4. Cross sectional images of porosity obtained by CT for core 1	24
5. Scanning electron microphotographs of diatomite pore structure: (a) before injection 1000X, 30 $\mu\text{m}$ arrow, (b) inlet after injection 1000X, 30 $\mu\text{m}$ arrow, and (c) inlet after injection 5000X, 6 $\mu\text{m}$ arrow	25
6. Average permeability versus time for cores 3 to 6	26
7. Average cross-sectional porosity, cores 2 to 6.	27

## **Acknowledgements**

Financial support was provided by the Stanford University Petroleum Research Institute. This paper was prepared with the support of the U.S. Department of Energy, under Award No. DE-FC26-00BC15311. However, any opinions, findings, conclusions, or recommendations expressed herein are those of the authors and do not necessarily reflect the views of DOE. Additionally, funding was provided by the SUPRI-A Industrial Affiliates and the President's Fund of Stanford University. This support is gratefully acknowledged.

We thank Mr Paul Hagin (Stanford Geophysics) for measuring the compressibility of our rock samples. Mr. Bob Jones (Stanford Geology and Environment Sciences) assisted with SEM imaging.

## **Abstract**

An experimental study of silica dissolution was performed to probe the evolution of permeability and porosity in siliceous diatomite during hot fluid injection such as water or steam flooding. Two competing mechanisms were identified. Silica solubility in water at elevated temperature causes rock dissolution thereby increasing permeability; however, the rock is mechanically weak leading to compression of the solid matrix during injection. Permeability and porosity can decrease at the onset of fluid flow. A laboratory flow apparatus was designed and built to examine these processes in diatomite core samples. At the core level, we measured the pressure drop as a function of time for fixed injection rates to determine permeability variation and utilized an X-ray Computerized Tomography (CT) scanner to measure in-situ porosity. At the pore level, a scanning electron microscope (SEM) was used to observe changes in pore morphology. We found that porosity decreased initially due to compaction caused by the imposed pressure drop across the core. Later, porosity increased as silica dissolved. Dissolution of the rock matrix appeared to be relatively uniform; wormholes were not observed even after tens of pore volumes of fluid injection.

## 1. INTRODUCTION

Diatomaceous rock is composed of biogenic silica, detritus, and shale in different proportions depending on its origin. The characteristics of this rock are high porosity (25-65%), rich in oil (35-70%), but low permeability (0.1 to 10 md) (Schwartz, 1988). Cumulatively, diatomaceous petroleum reservoirs in the San Joaquin Valley, California contain roughly 12 billion bbl of original oil in place (Ilderton *et al.*, 1996). The recovery of oil from diatomite by usual techniques is difficult because the permeability of diatomite is very low, compared to typical sandstone reservoirs. Thermal techniques have been tested for recovery of heavy and medium oil from diatomite in the South Belridge and Cymric fields (Kern Co., CA), and steam drive has been found to be technically successful (Kovscek *et al.*, 1997; Kumar and Beatty, 1995; Johnston and Shahin, 1995; Murer *et al.*, 2000). Steam injection, however, may lead to new complications because of rock dissolution and precipitation and the ensuing evolution of pore morphology (Koh *et al.*, 1996; Bhat and Kovscek, 1999). Additionally, relatively high injection pressures are necessary to force steam to enter a low-permeability rock matrix. This may lead to compaction or fracturing of the rock matrix in extreme cases.

Little is available in the literature in the way of previous experimental work regarding silica dissolution in diatomite. Prior work on the effects of dissolution and precipitation of reservoir solids, as related to oil recovery, is concerned mainly with acidizing of sandstones and carbonates, not the effect of hot water (*c.f.*, Williams *et al.*, 1979). Some acidizing principles clearly apply. For instance, selective dissolution of the solid matrix leads to the formation of "wormholes" as the dissolution rate relative to the interstitial velocity decreases (Hoefner and Fogler, 1988; Daccord *et al.*, 1993). Nonuniform dissolution along preferential paths of fluid flow occurs when convection is

dominant. Essentially, the large dimension flow space grows at a more rapid rate than small dimension flow space leading to the formation of large diameter channels referred to as “wormholes”. On the other hand, dissolution is nearly uniform when the process is reaction limited (Bekri *et al.*, 1995). Silica dissolution kinetics have been examined along with the migration of alkali in connection with alkaline waterflooding (Bunge and Radke, 1982). Generally, dissolution is not a first order reaction although it is frequently estimated as such. The evolution of grain shapes and sizes during dissolution was studied in permeable glass beadpacks (Udell and Lofy, 1989). Here, it was suggested that silica dissolution was most likely to occur uniformly along wetted surfaces.

Permeability-damage experiments in diatomite have been conducted by injecting silica-laden water and monitoring the reduction in permeability as the initial porosity fills with deposited solids (Koh *et al.*, 1996). The small grain size and small pore-throat sizes, as evidenced by low permeability, require only a small amount of precipitated solid to reduce effectively fluid mobility. Permeability reduction scales with porosity in a power-law fashion where the exponent is 9. Presumably, the increase in permeability with dissolution could be similarly drastic. In related work, a network model was proposed to gauge how evolving pore topology of diatomite affects permeability and porosity (Bhat and Kovscek, 1999). Network results agreed satisfactorily with the experiments of Koh *et al.* (1996).

This paper reports the construction of an isothermal laboratory apparatus to study dissolution accompanying one-dimensional fluid flow at a variety of flow rates and elevated temperatures. We intend to begin to unravel the evolution of porosity and permeability in diatomite. The effect of hot, fresh water is our focus because it is most relevant to steam condensation and resulting water flow near injection wells when steam is first injected into a cool formation.

Computerized tomography (CT) and scanning electron microscope (SEM) images are used to monitor experimental progress in addition to conventional measurement of permeability.

The next sections outline the apparatus and experimental procedure. Also discussed is the design and machining of the core holder. We then present the experimental results and compare them with theoretical predictions.

## 2. EXPERIMENTAL APPARATUS

A high-temperature apparatus, depicted schematically in Fig. 1, was designed and constructed. In some regards it is similar to the setup used by Koh *et al.* (1996), but it allows for measurement of porosity by CT scanning. A Blue-M oven, with precision temperature control, houses the coreholder and a high-pressure bomb for water supply. The bomb volume is  $0.0015 \text{ m}^3$  (1500 mL) and flow rates are low such that water injected into the bomb is heated to the oven set-point temperature. System pressure is elevated by a back-pressure regulator and injection occurs by pump.

For this work we use eight different core samples of diatomite all cut from a single outcrop block from the GREFCO Inc. quarry (Lompoc CA). Nominal initial permeability and porosity values are 4 mD and 0.67, respectively. These values agree well with previous measurements of this outcrop (Akin *et al.*, 2000). Core lengths were varied to satisfy particular values of dimensionless numbers as described later. All cores were cylindrical with a radius of 0.0125 m (1.25 cm). Cores 1 to 3 and 5 to 7 had a length of 0.09 m while core 4 had a length of 0.03 m.

An aluminum core holder, as shown in Fig. 2, was fabricated and cores were set in epoxy. The cores were first coated with a thin layer of epoxy to seal the surface. A test core was sawn in half to verify that epoxy penetration was less than 0.5 mm. After this layer dried, the cores were

potted in aluminum sleeves using epoxy resin 314 (TAP Plastics Inc. Dublin, CA) for cores 1 and 2, and with epoxy 4461 (COTRONICS Corp., NY) for the others. The second epoxy is rated to a temperature of 204 °C. Two holes were bored into the side of the 0.09 m long holders so that pressure could be measured along the length of the core. On either end of the core, endcaps contain spider-webbed shaped grooves to distribute flow evenly. The endcaps hold teflon o-rings for sealing against the face of the core holder. A large threaded ring holds the endcaps in place and provides compression to seal the o-rings. The o-rings protrude from the endcaps and seal against the aluminum portion of the coreholder such that the diatomite core is not compressed during assembly. The holder is designed for easy removal from the oven so that it can be mounted and scanned by X-ray CT for porosity evolution.

For water injection, we use two Isco 500D Series Syringe Pumps (ISCO, Lincoln, NE) ganged to operate in series. They provide continuous flow and low rates. For the experiments in cores 4 and 5 we use a classical reciprocating chromatographic pump. (ALTEX, model 100A).

Pressure drop is measured along the core using a quartz crystal transducer (Paroscientific Inc, Redmond,WA). A multiplexing valve enables this single transducer to make all pressure measurements. A Grove Mity-Mite backpressure regulator (Grove Valve and Regulator, Emeryville, CA) is used at the outlet of the core. We maintain system pressure greater than the saturation pressure of water, for a given temperature, to ensure that water remains liquid.

A Picker 1200SX Dual Energy X-ray Computerized Tomography (CT) scanner is used to measure porosity. The field size is 0.20 m. Our use of this machine and porosity measurement algorithms are described elsewhere (Akin *et al.*, 2000). The protocols used for these experiments include a voxel dimension of 0.25 mm by 0.25 mm by 10 mm, tube current and voltage of 200 mA

and 130 kV, respectively, and an exposure time of 6.79 s per slice. An X-ray filter was used to collimate the beam.

For examination of grain and pore structure in detail, an Hitachi S2500 model scanning electron microscope was used. In addition to its high power of magnification, an SEM image can be tilted to examine three-dimensional features. All samples were first sputtered with a gold-palladium coating to make surfaces electrically conducting.

### **3. EXPERIMENTAL PROCEDURE**

It is difficult to conduct laboratory experiments precisely at reservoir conditions. Thus, we used appropriate dimensionless numbers to guide experimental parameter selection. This section discusses our choices of experimental temperatures and flow rates, experimental procedure, and data analysis. Silica deposition was not expected in this work because fresh water was injected and the experimental temperature was maintained constant. There was no opportunity for deposition.

#### **3.1 Design**

The relevant dimensionless parameters for the dissolution process are the Peclet,  $Pe$ , and Damkohler,  $Da$ , numbers (*c.f.*, Bekri *et al.*, 1995; Bhat and Kovscek, 1999). The Peclet number is the ratio of the characteristic time for diffusion upon time for convection, while the Damkohler number is the ratio of the characteristic time for fluid convection upon the time for dissolution. The product of  $Pe$  and  $Da$  numbers is the important scaling parameter (Bekri *et al.*, 1995). If this product,  $PeDa$ , is less than 1 the process is reaction limited and dissolution is nearly uniform. On the other hand, the process is transport limited for  $PeDa$  greater than 1, and the formation of wormholes is expected.

The magnitude of PeDa permitted us to scale conditions so as to be field relevant. The dimensionless Peclet and Damkholer (assume first order reaction) numbers are defined, respectively, by

$$Pe = \frac{vd}{D} \quad (1a)$$

$$Da = \frac{L\kappa}{v} \quad (1b)$$

where  $v$  is a characteristic velocity taken here as the mean interstitial velocity,  $d$  is a characteristic dimension,  $D$  is the solute diffusivity,  $L$  is a characteristic length, and  $\kappa$  is a first-order rate constant. The characteristic dimension in Pe is appropriately a pore size (*e.g.*, diameter) because pores are the conduits carrying flow in porous media; the appropriate characteristic dimension in Da is core length because reaction occurs along its entire length. From Eq. (1), we have

$$PeDa = \frac{\kappa Ld}{D} \quad (2)$$

The reaction models of Koh *et al.* (1996) and Rimstidt and Barnes (1980) are used to estimate  $\kappa$

$$\kappa_1 = 1.1 \times 10^{-4} \exp\left(\frac{1192}{T}\right) \quad (3a)$$

$$\kappa_2 = \frac{(1-\phi)\rho_r S_v}{\phi\rho_w} 10^{-0.707 - \frac{2598}{T}} \quad (3b)$$

where the subscripts 1 and 2 refer to Koh *et al.* and Rimstidt and Barnes expressions, respectively,  $\phi$  is the porosity,  $S_v$  is the specific surface area of diatomite, the product  $(1-\phi)\rho_r$  is the bulk density of diatomite,  $\rho_w$  is the liquid density, and  $T$  is the absolute temperature in Kelvin.

In our study, we injected liquid water and maintained the system backpressure at a level sufficiently high to avoid vaporization. Table 1 summarizes the conditions for each experiment. We assume  $\phi$  equals 0.65, a bulk rock density (Schwartz, 1988; Stosur and David, 1971) of 880 kg/m<sup>3</sup>,  $S_v$  of 20,000 m<sup>2</sup>/kg (Bruton, 1997), and draw liquid water density from the steam tables (Weast, 1983) to obtain numerical values from Eqs. (1) to (3). For the characteristic length,  $L$ , we choose core length. We set the characteristic pore dimension,  $d$ , equal to  $\sqrt{k/\phi}$  with the permeability,  $k$ , set to the nominal value of 4 mD.

According to the two different expressions for reaction rates and values of PeDa, we expect uniform dissolution even at elevated temperature. Field values of PeDa for hot fluid injection into diatomite should also be less than 1 for temperatures less than 200°C (392 °F) and the parameters given above. Such temperature ranges have been reported for at least two projects (Kovscek *et al.* 1997; Murer *et al.* 2000).

### 3.2 Procedure

The porosity of each core was measured before injection began and periodically during an experiment. It is necessary to scan the core completely dry and then completely saturated with water to calculate porosity. The core is dried by placing it in a vacuum oven at 70°C for at least 12 hours. After the dry scans are complete, water is imbibed co-currently for at least two hours followed by injection of gas-free water to remove any residual gas. Due to large capillary pressure, imbibition is rapid even though permeability is low. This procedure proved successful to saturate

fully cores in previous work (Akin *et al.*, 2000). The drying and saturating procedure was the same for all experiments.

To obtain a precise map of porosity along the length of the core, scans were made at 0.01 m intervals in the direction of flow. Then the core was placed in the oven, water was injected at constant flow rate as indicated in Table 1, and the oven brought to the desired temperature. We assume that the water stays in the liquid state as long as pressure is greater than the saturation pressure for a given temperature. At least 20 PV were injected for each experiment and in some cases over 200 PV were injected. Periodically, injection was stopped, the system cooled, the core removed from the oven, and porosity measured by scanning at the same positions as used initially (repositioning to within  $\pm 1$  mm). This required new wet and dry scans in order to capture the change in porosity and to negate positioning errors. The number of porosity measurements as a function of time are relatively few because the oven had to be turned off and the core removed in order to make measurements. Pressure measurements were made frequently throughout the duration of the experiment.

### 3.3 Analysis

The porosity is deduced from the CT numbers measured during each scan. We calculate the porosity as (Withjack, 1988)

$$\phi = \frac{CT_{cw} - CT_{cd}}{CT_w - CT_a} \quad (4)$$

where  $CT_{cw}$  is the CT number for a 100% water saturated core,  $CT_{cd}$  is the CT number for a dry core, and  $CT_w$  and  $CT_a$  refer to water and the air phases, respectively. In this manner, we obtain

voxel by voxel measurements of porosity. Average porosity is found by averaging over a slice and then averaging all slices if average core porosity is desired.

The permeability of the core is computed using Darcy's Law, the measured pressure drop, and the known injection rate according to

$$k = \frac{Ql}{A\Delta p} \mu_w \quad (5)$$

where  $k$  is the rock permeability,  $\mu_w$  viscosity of water as a function of temperature,  $\Delta P$  pressure difference,  $l$  distance between pressure taps, and  $A$  cross-sectional area.

#### 4. EXPERIMENTAL RESULTS

The experimental measurements are permeability, porosity, and images of pore structure. We consider the results from the first experiment in some detail because they are, generally, representative of all experiments. Figure 3 displays the permeability and porosity evolution for water injection at 80°C and a frontal advance rate of 0.59 m/d (0.201 cm<sup>3</sup>/min). On the left, the permeability measured between the various sections of the core is reported. Note that initial permeability is a little more than 4 mD and is uniform over the core. Permeability drops by a factor of 2 to 4 within the first pore volume of fluid injection. The largest drops in permeability are found in the sections nearest the outlet. On the right of Fig. 3 is the average porosity measured at 0.01 m (1 cm) intervals along the length of the core. Upon examination of porosity profiles at times of 0 PV and 16.5 PV, it is found that porosity decrease accompanied the decrease in permeability.

Following the initial decrease in permeability, the average permeability of the core increased slowly and more dramatically between the inlet and the first pressure tap. As reported on Fig. 3,

permeability recovered at a rate of about 0.01 mD/PV. The porosity profiles at 31.5 and 51.5 PV indicate that porosity generally increased during this later period.

The pattern of porosity change observed in CT images is uniform and subtle. Figure 4 presents the CT images of porosity from which the average porosities in Fig. 3 were computed. Black corresponds to a porosity of 0.5 while white signifies 1. Note that the shading within each image does not vary substantially indicating uniform dissolution of the rock matrix, as expected from the magnitude of PeDa. Even after much injection, the regions near the inlet display nearly uniform porosity within each cross section. In all experiments nearly uniform porosity is measured within a given cross section at all times; hence, we summarize CT measurements as porosity values averaged over the cross section.

SEM images of diatomite grain structure were collected from samples of the cores before and after flooding stopped. Figure 5 gives three of these images. Note in Fig. 5a the magnification is 1000X and a length scale of 30  $\mu\text{m}$  is indicated in the lower right corner by a double-headed arrow. This outcrop sample consists largely of diatom fragments, although it is relatively easy to find intact and partially-intact diatoms. Prior to injection, a variety of fragments sizes are visible and fragment edges are relatively sharp. Figures 5b and 5c display images of samples drawn from the inlet of core 1 after injection was complete. Figure 5b is again at a magnification of 1000X while Fig. 5c was acquired at 5000X. The image in Fig. 5b appears to be little changed relative to Fig. 5a. The major difference lies in the sharpness of grain edges. Figure 5c is an enlargement of the central portion of Fig. 5b. Smoothing of the sharp edges of diatomite fragments is evident. Such dissolution of rock is responsible for the slow increase in permeability witnessed in Fig. 3.

The trends in permeability and porosity evolution exhibited by the first experiment were generally repeated in the subsequent experiments. Figure 6 presents the average permeability for

Experiments 3 to 7. Initial permeability is in the neighborhood of 4 mD and then drops to 1 or 2 mD after the hot water begins to flow. At later times, permeability increases slowly with injected volume. Exact values of the rate of increase are given on Fig. 6. Due to a failure of the scanning valve, no pressure data were collected for experiment 2. Figure 7 gives the corresponding porosity profiles for each experiment. All experiments display a decrease in porosity following the start of injection. In Experiments 2, 3, and 4, conducted at 80°C, the porosity at later times (*e.g.*, 50 PV) always remains less than the initial. In Experiments 5 and 6, conducted at 121 °C, the porosity at later times surpasses the initial values. These experiments also exhibit the largest increases in permeability because the solubility of silica increases with temperature. No porosity information was collected for experiment 7.

In summary, a strong effect of compression of the rock samples is witnessed in both measured permeability and porosity. Permeability of the samples increases slowly once the rock is compressed because of dissolution of the rock matrix. Through inspection of cross sections of porosity, we find that dissolution is uniform, as expected from the scaling analysis.

## 5. DISCUSSION

The porosity of cores did not increase uniformly from the start of injection. Previous work considering compaction of diatomaceous rock (opal A) reported overall pore volume compressibility,  $C_{pv}$ , ranging from 70 to 170  $\mu\text{sips}$  ( $1 \mu\text{sip} = 1 \times 10^{-6} \text{ psi}^{-1} = 16.6 \times 10^{-6} \text{ kPa}^{-1}$ ) (Chase and Dietrich, 1989; Bowersox and Shore, 1990; Wendel *et al.*, 1988). A simple equation for the effect of compressibility on porosity is (Chase and Dietrich, 1989; Zuber *et al.*, 1987)

$$\phi = \phi_o \exp[C_{pv}(p_o - p)] \quad (6)$$

where the subscript  $o$  on  $\phi$  and  $p$  indicates initial values. Equation (6) predicts reduction in porosity from 1 to 2% with the above values of  $C_{pv}$  and overall pressure differences of roughly 50 psi (690 kPa) that are representative of these experiments. Indeed, we chose to work at relatively low temperatures of 80 and 121°C to avoid the imposition of large backpressure that would induce compression of the solid matrix during pressurization of the system.

To attempt to explain the discrepancy between predicted and measured reductions in porosity, rock compressibility and compaction coefficient were measured for virgin samples of the experimental core material. Samples are compressed by establishing a constant pore pressure and then increasing the confining pressure, hence, the effective pressure. Details of the apparatus are given by Chang and Zoback (1998). Results yield an overall pore volume compressibility of 170  $\mu$ sips (average of two samples). This compares favorably with previous measurements. However, it should be noted that describing these samples with a single constant compressibility is simplistic as the measured strain exhibited a fair degree of creep while the effective pressure was held constant. That is, there is a degree of time lag to changes in pore pressure.

The apparent overall pore-volume compressibility exhibited in the flow experiments can be computed from the porosity data and Eq. (6). Table 2 summarizes the calculations. Porosity is averaged over the entire core and the average is indicated by  $\bar{\phi}$ . We calculate  $C_{pv}$  from the initial and first average porosity measured after the start of injection. Note that the apparent pore-volume compressibilities are roughly an order of magnitude larger than the literature values and our measurement of compressibility under no-flow conditions. The effect of compression on

permeability is also summarized in Table 2. From the simple porosity-permeability relationship

$$k = k_o \left( \frac{\phi}{\phi_o} \right)^\gamma \quad (7)$$

and the permeability data in Fig. 6, the value of the exponent  $\gamma$  can be calculated. Except for experiment 4, we obtain a consistent value of 5 to 6 for  $\gamma$  indicating the strong effect of compression of the matrix on permeability. In experiment 4, either the initial permeability or that after compression appears to be in error rather than the measurement of porosity. Previous work regarding silica deposition in diatomite for the injection of hot silica laden water into cold rock established the applicability of Eq. (7) and values of  $\gamma$  in the range of 8 to 9 were found (Koh *et al.*, 1996; Bhat and Kovscek, 1999). Thus, the effect of compression in the experiments reported here is not as dramatic as the plugging of pore space with precipitated solid.

The difference between the apparent pore-volume compressibilities exhibited within the experiments and the values in the literature may be linked to the flow through nature of our experiments. The samples are only weakly consolidated as demonstrated by the fact that they can be shaped with files and sandpaper. Flow may aid the rearrangement of grains or other fine rock material and contribute to the large apparent compressibility. Fines mobilization has been noted in some sandstone systems and attributed to the colloidal nature of fine particles (Tang and Morrow, 1999). In conventional compressibility measurements of rock samples, the pore pressure is fixed and then the confining pressure is increased or decreased. Thus, there is no bulk flow of the pore fluid.

Figure 6 indicates that the restoration of permeability due to dissolution of the rock matrix is not dramatic and very slow. In light of the strong correlation between reduction in porosity and

permeability, we expected permeability to increase substantially during Experiments 5 and 6 because the porosity after 20 to 30 PV of injection is about equal to the initial value. Once these samples are compressed, however, recovery of permeability is nearly irreversible and does not correlate strongly with porosity.

The lack of a strong increase in permeability with a large increase in porosity indicates that pore bodies and other large features dissolve more quickly than pore throats or similar constrictions in the path of flow. This situation could arise because of continual mobilization or shifting of the smallest grains. As a result, pore throats are persistently reblocked with new material when dissolution at a pore throat occurs. Nevertheless, the trends reported at late time (greater than 4 PV) in Fig. 6 indicate that net dissolution of the rock matrix does result in slow and steady increases in permeability. Because the size of constrictions to flow increases slowly, the permeability increases slowly.

## **6. CONCLUSIONS**

The results of this experimental investigation show that for some conditions of hot-water injection diatomite undergoes a reduction in porosity and permeability due to flow-induced compression and rearrangement of rock-mineral grains. The effects of this compression here were more severe than indicated by previous examinations of diatomite compressibility. In some cases, a roughly three-fold reduction in permeability was witnessed. Dissolution of the rock matrix is a slow process relative to compression and cannot compensate for reduction in permeability until very many pore volumes of fluid are injected. Based upon the results reported here, it would appear to be beneficial to consider the role of rock compression whenever hot fluid is injected into diatomite.

The pattern of dissolution observed by CT scans, SEM images, and visual inspection of cores is uniform dissolution of the rock matrix. No evidence of wormholes or other selective dissolution phenomena was witnessed. These observations concur with previous theoretical analyses of the dissolution of porous media.

## Nomenclature

$A$  = cross-sectional area

$C_{pv}$  = pore-volume compressibility

CT = CT number

$d$  = characteristic pore dimension

$D$  = diffusivity

Da = Damkholer number

$k$  = permeability

$L$  = characteristic length

$p$  = pressure

Pe = Peclet number

$Q$  = volumetric flow rate

$S_v$  = specific surface area of diatomite

$T$  = temperature

$v$  = interstitial velocity

## *Greek letters*

$\phi$  = porosity

$\kappa$  = rate constant

$\mu$  = viscosity

$\rho$  = density

*Subscripts and Superscripts*

1,2 denote rate constant models

*a* denotes air

*cd* denotes a dry core

*cw* denotes water saturated core

*o* denotes an initial value

*r* denotes rock

*w* denotes water

## References

1. Akin, S., J.M. Schembre, S.K. Bhat, and A.R. Kovsky. 2000. Spontaneous Imbibition Characteristics of Diatomite. *J. Pet. Sci. & Eng.* 25: 149-165.
2. Bekri, S., J.F. Thovert, and P.M. Adler. 1995. Dissolution of Porous Media. *Chem. Eng. Sci.* 50 : 2765-2791.
3. Bhat, S.K. and A.R. Kovsky. 1999. Statistical Network Theory of Silica Deposition and Dissolution in Diatomite. *In Situ.* 23: 21-53.
4. Bowersox, J.R. and R.A. Shore. 1990. Reservoir Compaction of the Belridge Diatomite and Surface Subsidence, South Belridge Field, Kern County, CA in *Structure, Stratigraphy and Hydrocarbon Occurrences of the San Joaquin Basin, California*, J.G. Kuespert and S.A. Reid, Editors. , The Pacific Section, Society of Economic Paleontologists and Mineralogists and the American Association of Petroleum Geologists, Bakersfield, CA. p. 225-230.
5. Bruton, C. 1997. Personal Communication.
6. Bunge, A.L. and C.J. Radke. 1982. Migration of Alkaline Pulses in Reservoir Sands. *Soc. Pet. Eng. J.* 22: 998-1012.
7. Chang, C. and M. D. Zoback. 1998. Viscous Rheology and the State of Stress in Unconsolidated Sands in SPE/ISRM Rock Mechanics in Petroleum Engineering, Society of Petroleum Engineers, Richardson, TX. p. 465-474.
8. Chase, C.A.Jr. and J.K. Dietrich. 1989. Compaction Within the South Belridge Diatomite. *Soc. Pet. Eng. Res. Eng.* Nov. 422-428.
9. Daccord, G., O. Lietard, and R. Lenormand. 1993. Chemical Dissolution of a Porous Medium by a Reactive Fluid--II. Convection vs. Reaction, Behavior Diagram. *Chem. Eng. Sci.* 48 : 179-186.
10. Hoefner, M.L. and H.S. Fogler. 1988. Pore Evolution and Channel Formation During Flow and Reaction in Porous Media. *AIChE J.* 34 : 45-54.
11. Ilderton, D.C., T.W. Patzek, J.W. Rector, and H.J. Vinegar. 1996. Passive Imaging of Hydrofractures in the South Belridge Diatomite. *Soc. Pet. Eng. Form. Eval.* Mar: 46-54.
12. Johnston, R.M. and G.T. Shahin. 1995. Interpretation of Steam Drive Pilots in the Belridge Diatomite. SPE 29621. Proceedings of the SPE 65th Western Regional Meeting, Bakersfield, CA March 8-10.
13. Koh, C.J., P.C. Dagenais, D.C. Larson, and A.S. Murer. 1996. Permeability Damage in Diatomite Due to In-situ Silica Dissolution/Precipitation. SPE 35394. Proceedings of the SPE/DOE Tenth Symposium on Improved Oil Recovery, Tulsa, OK April 21-24.

14. Kovscek, A.R., R.M. Johnston, and T.W. Patzek. 1997. Evaluation of Rock/Fracture Interactions During Steam Injection Through Vertical Hydraulic Fractures. *Soc. Pet. Eng. Prod. and Facilities*. May: 100-105.
15. Kumar, M. and F.D. Beatty. 1995. Cyclic Steaming in Heavy Oil Diatomite. SPE 29623. Proceedings of the SPE 65th Western Regional Meeting, Bakersfield, CA March 8-10.
16. Murer, A.S., K.L. McClennen, T.K. Ellison, D.C. Larson, R.S. Timmer, M.A. Thomsen, K.D. Wolcott. 2000. Steam Injection Project in Heavy Oil Diatomite. *Soc. Pet. Eng. Res. Eng. and Eval.* Feb: 2-12.
17. Rimstidt, J.D. and H.L. Barnes. 1980. The Kinetics of Silica Water Reactions. *Geochim. Cosmochim. Acta* 44: 1683-1699
18. Schwartz, D.E. 1988. Characterizing the Lithology, Petrophysical Properties, and Depositional Setting of the Belridge Diatomite, South Belridge Field, Kern County, California in *Studies of the Geology of the San Joaquin Basin*, S.A. Graham, and Olson, H.C., Editors. The Pacific Section, Society of Economic Paleontologists and Mineralogists, Los Angeles . p. 281-301.
19. Stosur, J.J. and A. David. 1971. Petrophysical Evaluation of the Diatomite Formation of the Lost Hills Field, California. *Jour. Pet. Tech.* 28: 1138-1144.
20. Tang, G-Q. and N.R. Morrow, 1999. Influence of Brine Composition and Fines Migration on Crude Oil/ Brine/ Rock Interactions and Oil Recovery, *J. Pet. Sci. & Eng.*, 24: 99-111.
21. Udell, K.S. and J.D. Lofy. 1989. Permeability Reduction of Unconsolidated Media Caused by Stress-Induced Silica Dissolution. *Soc. Pet. Eng. Form. Eval.* Mar: 56-62.
22. Weast, R.C., editor, 1983. CRC Handbook of Chemistry and Physics., CRC Press, Boca Raton, FL.
23. Wendel, D.J., L.A. Kunkel, and G.S. Swanson. 1988. Waterflood Potential of Diatomite: New Laboratory Methods. SPE 17439. Proceedings of the SPE California Regional Meeting, Long Beach, CA Mar. 23-25.
24. Williams, B.B., J.L. Gidley, and R.S. Schechter. 1979. *Acidizing Fundamentals*. Society of Petroleum Engineers of AIME, Dallas, TX.
25. Withjack, E.M. 1988. Computed Tomography for Rock Property Determination and Fluid Flow Visualization. *Soc. Pet. Eng. Form. Eval.* Dec: 696-704.
26. Zuber, M.D., W.K. Sawyer, R.A. Schraufnagel, and V.A. Kuuskraa. 1987. The Use of Simulation and History Matching To Determine Critical Coalbed Methane Reservoir Properties. SPE/DOE 16420. Proceedings of the SPE/DOE Low Permeability Reservoirs Symposium, Denver, CO May 18-19.

Table 1: Summary of Experimental Conditions

	$L(m)$	$T(^{\circ}C)$	Rate ( $cm^3/min$ )	Pe	Da(Koh/Rimstidt)	PeDa(Koh/Rimstidt)
1	0.09	80.0	0.201	0.00044	44/3.3	0.020/0.0015
2	0.09	80.0	0.201	0.00044	44/3.3	0.020/0.0015
3	0.09	80.0	0.201	0.00044	44/3.3	0.020/0.0015
4	0.03	80.0	0.330	0.00074	8.8/0.66	0.0066/0.00049
5	0.09	121.1	0.330	0.00074	19/12	0.014/0.0089
6	0.09	121.1	0.201	0.00044	31/20	0.014/0.0089
7	0.03	121.1	0.201	0.00044	10/6.6	0.0056/0.0030

Table 2: Summary of Apparent Compressibility From Flow Experiments

	Total $\Delta P(psi, kPa)$	$\bar{\phi}_o$	$\bar{\phi}(t)$	$C_{PV}(psi^{-1}, kPa^{-1})$	$\gamma$
1	280.0, 193	0.681	0.590 (16.5 PV)	$5.07 \times 10^{-3}, 7.35 \times 10^{-4}$	5.3
3	29.2, 201	0.720	0.621 (5 PV)	$5.07 \times 10^{-3}, 7.35 \times 10^{-4}$	4.6
4	20.5, 141	0.714	0.667 (5 PV)	$3.29 \times 10^{-3}, 4.77 \times 10^{-4}$	18
5	57.1, 394	0.659	0.546 (22 PV)	$3.31 \times 10^{-3}, 4.80 \times 10^{-4}$	4.6
6	61.6, 425	0.642	0.559 (13 PV)	$2.25 \times 10^{-3}, 3.26 \times 10^{-4}$	6.2

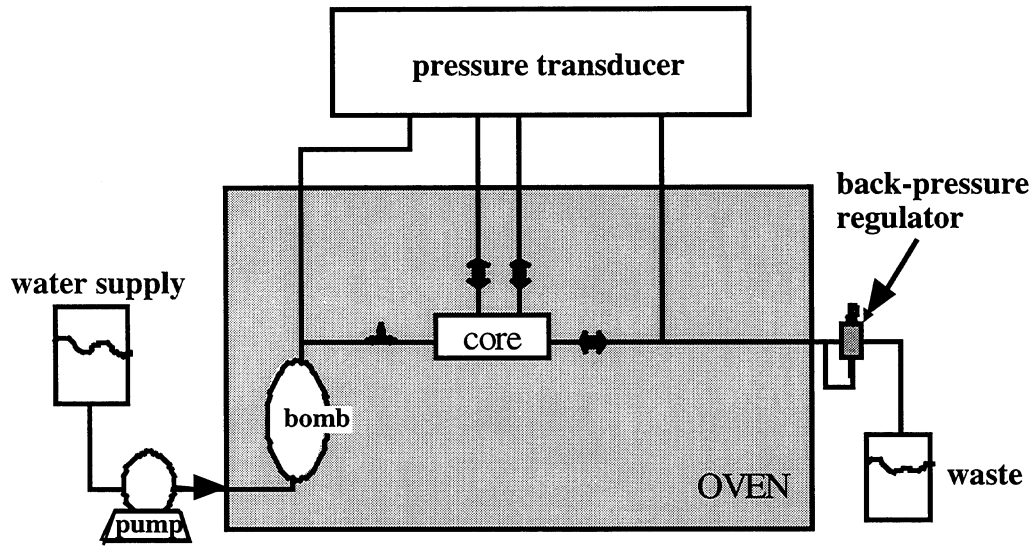


Figure 1. Schematic of experimental apparatus.

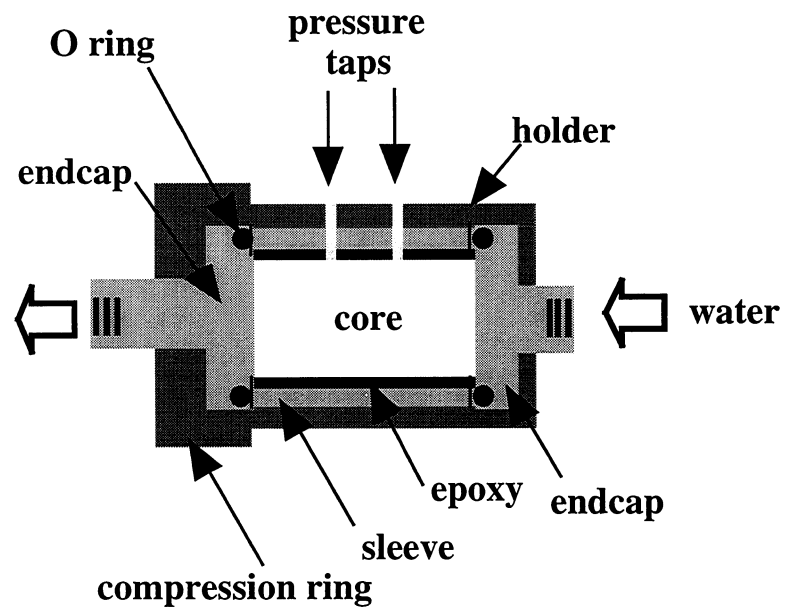


Figure 2. Schematic of core assembly.

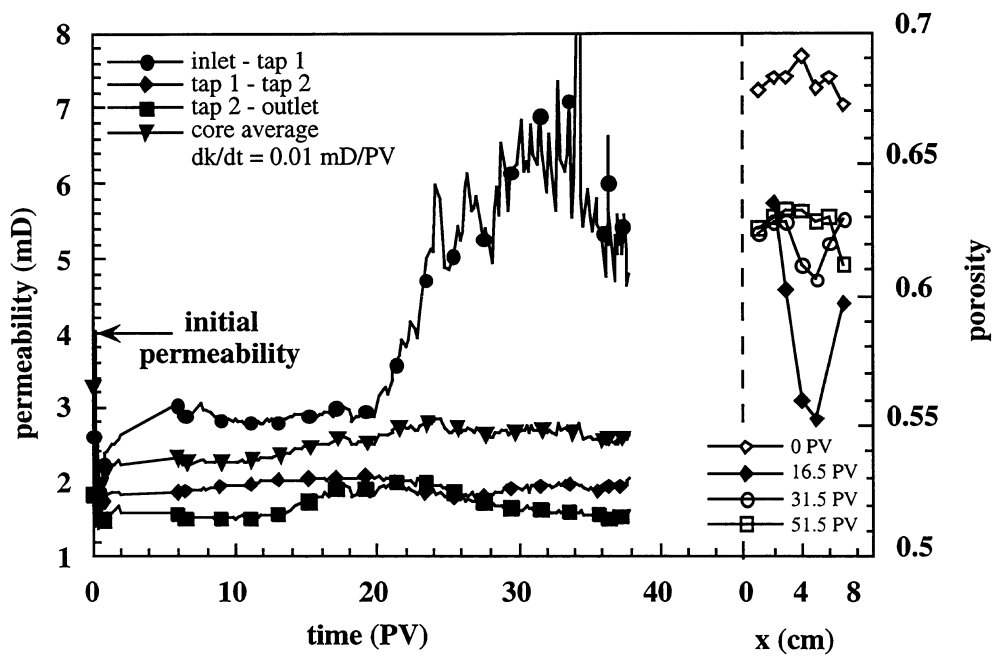


Figure 3. Permeability versus time (left) and porosity profiles (right) for core 1.

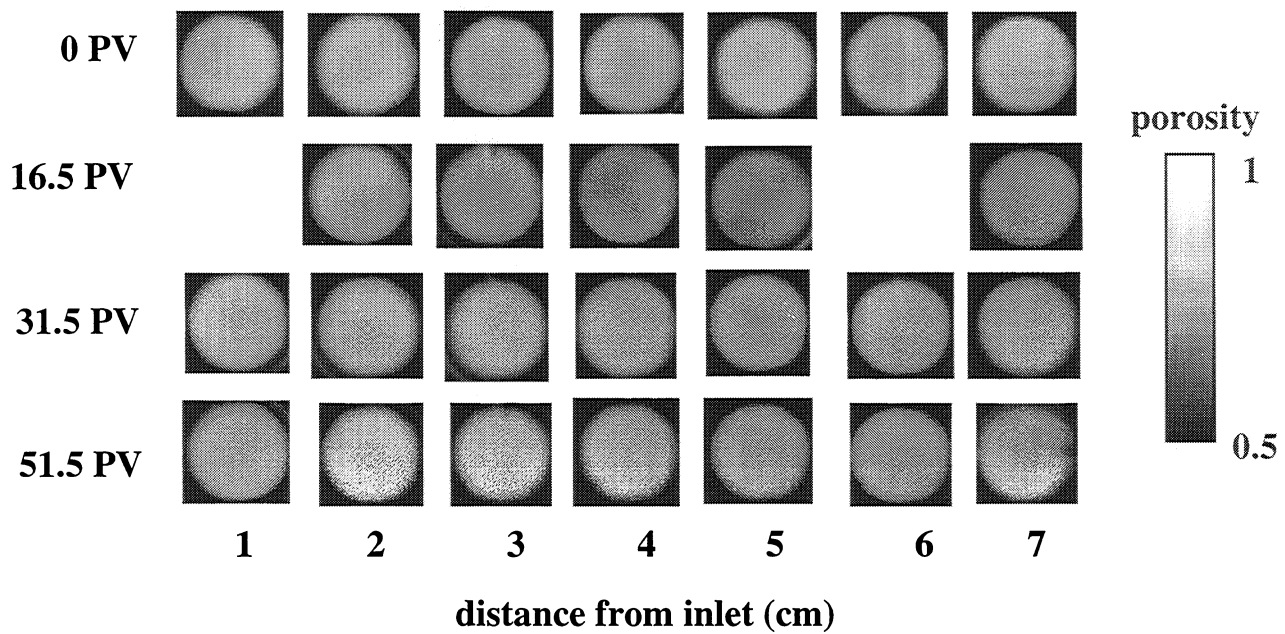


Figure 4. Cross sectional images of porosity obtained by CT for core 1.

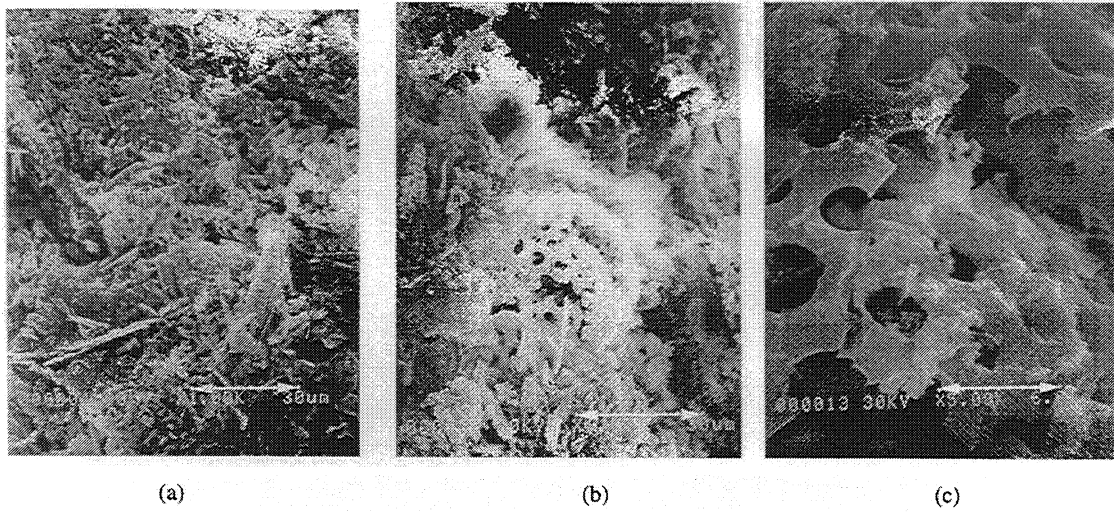


Figure 5. Scanning electron microphotographs of diatomite pore structure: (a) before injection 1000X, 30  $\mu\text{m}$  arrow, (b) inlet after injection 1000X, 30  $\mu\text{m}$  arrow, and (c) inlet after injection 5000X, 6  $\mu\text{m}$  arrow.

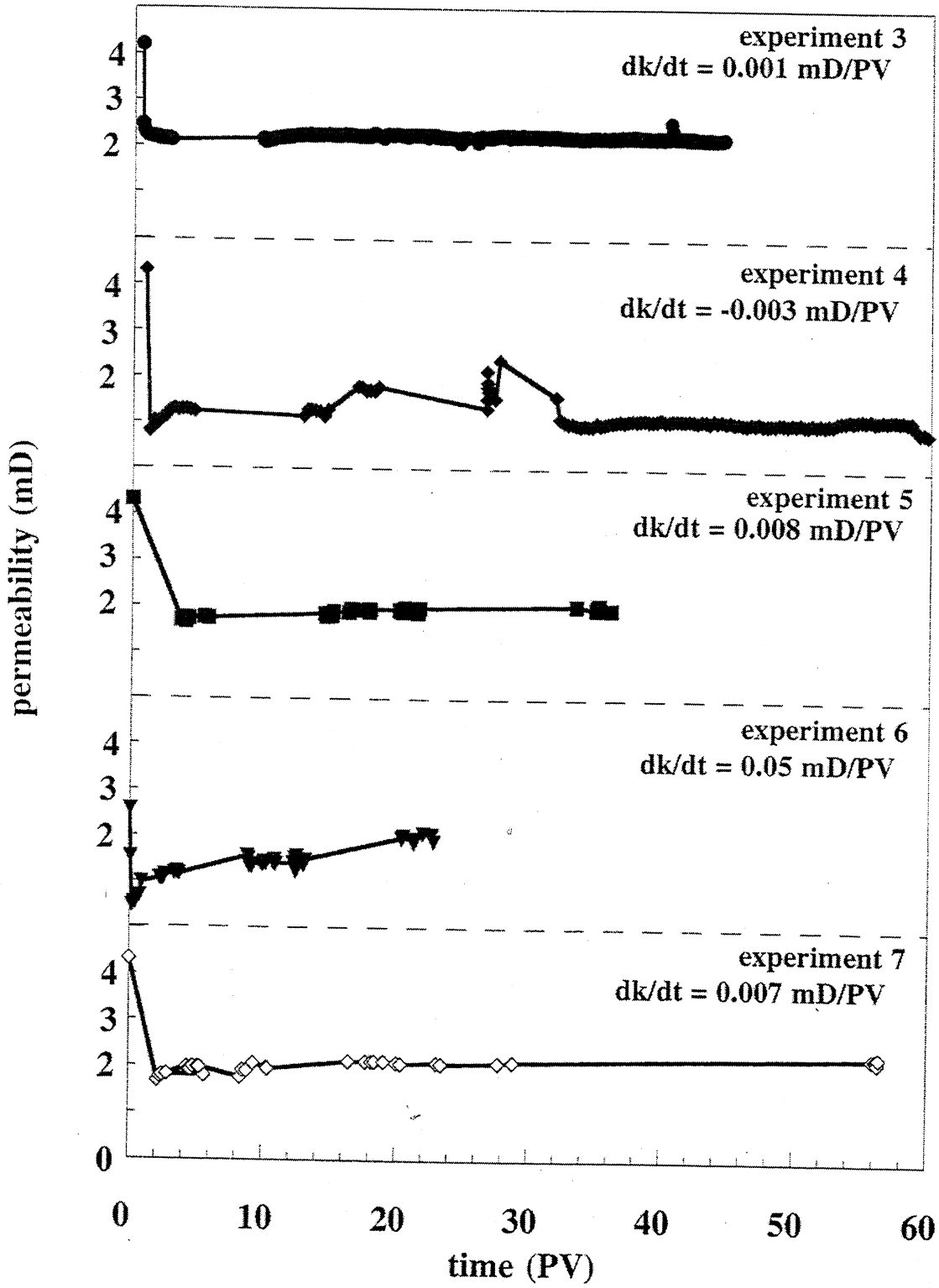


Figure 6. Average permeability versus time for cores 3 to 6.

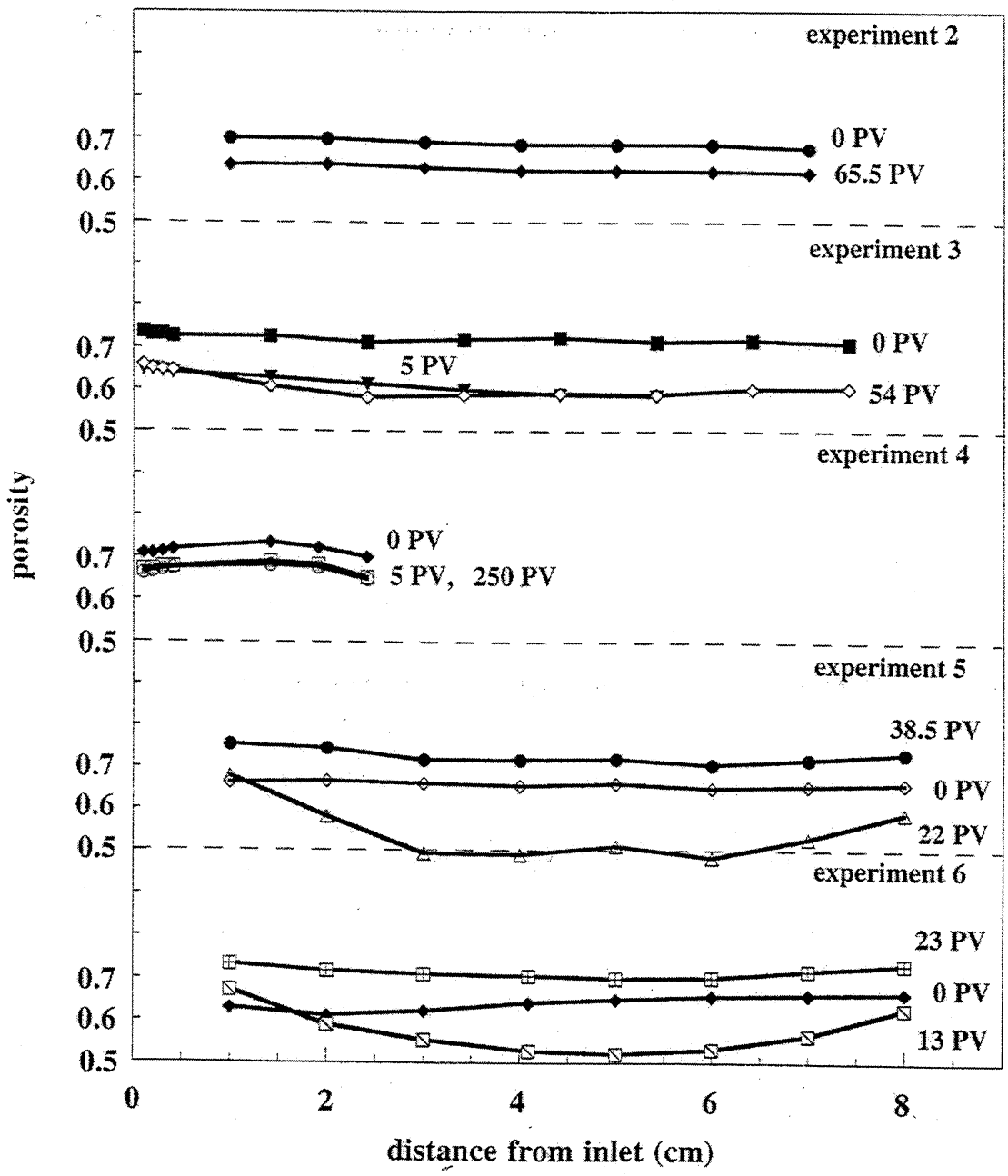


Figure 7. Average cross-sectional porosity, cores 2 to 6.

